# Progress Toward Spatially-Entangled Photon-Pair Generation in a Few-Mode Fiber

Afshin Shamsshooli<sup>®</sup>, Student Member, IEEE, Cheng Guo<sup>®</sup>, Graduate Student Member, IEEE, Francesca Parmigiani, Senior Member, IEEE, Xiaoying Li<sup>®</sup>, Member, IEEE, and Michael Vasilyev<sup>®</sup>, Senior Member, IEEE

Abstract—We describe a scheme for generation of spatial-mode-entangled photon pairs in a few-mode fiber and experimentally demonstrate generation of idler beams from classical seed signals representing various superpositions of fiber  $LP_{01}$  and  $LP_{11a}$  modes. For every signal mode superposition, we observe the indication of idler mode orthogonality to the signal mode.

*Index Terms*—Nonlinear fiber optics, inter-modal four-wave mixing, few-mode fibers, quantum communication, quantum entanglement, quantum information processing.

#### I. Introduction

NTANGLEMENT in multiple degrees of freedom, e.g., Lin polarization, frequency, time-bin, and spatial modes has a potential for carrying larger amounts of quantum information, which is important for quantum communication and information processing. While polarization, frequency, and time-bin entanglement generation has already been implemented in integrated form compatible with low-loss transport over optical fiber, the spatial entanglement still relies on bulk-crystal-based setups [1]. The spatially- or orbital-angularmomentum- (OAM) entangled photons have been generated in crystal platforms and transported over various media: turbulent free-space [2], hollow-core photonic crystal fiber [3], a few-mode fiber (FMF) [4]-[6], and vortex fiber [7]. As a possible alternative to crystal platform, FMF is gaining traction for making nonlinear devices based on inter-modal four-wave mixing (IM-FWM), owing to FMF's wide options for modeand dispersion-engineering, and excellent mode match to the FMFs used in low-loss transmission links [8]-[10]. Correlated photon pairs [11]-[13] and hybrid entanglement between frequency and spatial modes [14] were recently generated in FMFs by IM-FWM, but no attempts of generating spatial-mode entanglement through IM-FWM have

Manuscript received April 15, 2021; revised June 10, 2021; accepted June 10, 2021. Date of publication June 15, 2021; date of current version July 29, 2021. This work was supported in part by the NSF under Grant ECCS-1937860 and Grant ECCS-1842680. (Corresponding author: Afshin Shamsshooli.)

Afshin Shamsshooli, Cheng Guo, and Michael Vasilyev are with the Department of Electrical Engineering, University of Texas at Arlington, Arlington, TX 76019 USA (e-mail: afshin.shamsshooli@mavs.uta.edu; cheng.guo@mavs.uta.edu; vasilyev@uta.edu).

Francesca Parmigiani is with Microsoft Research, Cambridge CB1 2FB, U.K. (e-mail: francesca.parmigiani@microsoft.com).

Xiaoying Li is with the College of Precision Instruments and Opto-Electronics Engineering, Tianjin University, Tianjin 300072, China (e-mail: xiaoyingli@tju.edu.cn).

Color versions of one or more figures in this letter are available at https://doi.org/10.1109/LPT.2021.3089537.

Digital Object Identifier 10.1109/LPT.2021.3089537

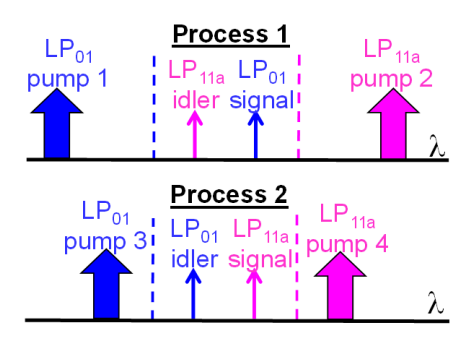


Fig. 1. Two parametric processes, whose combination enables generation of spatial-mode-entangled signal-idler photon pairs in the TMF.

been reported yet. We have recently introduced a novel scheme for generation of spatial-mode-entangled photon pairs directly in the FMF using a combination of two IM-FWM processes [15]. Using classical seed signals, we experimentally measured signal-idler mode selectivity separately for these two processes. In the present paper, we further combine both processes together and observe that they couple the input two-mode seed signal to an orthogonal two-mode idler for various signal-mode superpositions. This paper is an extended version of our recent IPC conference paper [16], providing more details on the background theory, experimental setup, and measurement procedures, as well as adding graphs demonstrating the mode selectivity for both IM-FWM processes involved.

# II. THEORY OF $\chi^{(3)}$ -BASED SPATIAL-MODE

Our spatial-mode entanglement scheme employs a combination of two IM-FWM processes of Fig. 1. We use an elliptical-core FMF [8] that supports three non-degenerate modes (LP<sub>01</sub>, LP<sub>11a</sub>, and LP<sub>11b</sub>), to be referred to as three-mode fiber (TMF) below. In IM-FWM process 1, with the help of pumps 1 and 2 a signal photon is created in mode LP<sub>01</sub> at frequency  $v_S$ , while idler photon is created in mode  $LP_{11a}$  at frequency  $v_I$ . In process 2, their roles interchange: in the presence of pumps 3 and 4, signal photon at frequency  $v_S$  is created in mode LP<sub>11a</sub>, whereas the idler photon at frequency  $v_I$  is created in mode LP<sub>01</sub>. With all 4 pumps present, both processes take place simultaneously. In the perfectly phase-matched regime at low pump powers (our case), both the classical signal-to-idler conversion efficiency (CE) and the probability of a single pair generation in each process are given by  $\langle n \rangle = g - 1 = \sinh^2[2\gamma (P_p P_q)^{1/2} L] \approx 4\gamma^2 P_p P_q L^2 \ll 1$ ,

1041-1135  $\odot$  2021 IEEE. Personal use is permitted, but republication/redistribution requires IEEE permission. See https://www.ieee.org/publications/rights/index.html for more information.

where L is the fiber length,  $P_{p(q)}$  is the pump power of mode p(q), g is the parametric gain, and  $\gamma = n_2\omega/(cA_{\rm eff})$  is the nonlinear constant, with  $A_{\text{eff}}$  being the effective area of the nonlinear interaction, equal to the inverse of the intensity overlap integral between the modes p and q. We require  $\langle n \rangle \ll 1$ to ensure that the probability of simultaneous generation of two pairs  $\langle n \rangle^2 \ll \langle n \rangle$  is negligibly small. The probabilities of pair generation in processes 1 and 2 can be equalized by adjusting relative powers of the two pump pairs, which leads to generation of the maximally-entangled state  $|LP_{01}\rangle_S |LP_{11a}\rangle_I +$  $e^{i\varphi}|LP_{11a}\rangle_S|LP_{01}\rangle_I$ , where phase  $\varphi$  can be changed by varying the pump phase difference  $\Delta \varphi = (\varphi_{P1} + \varphi_{P2}) - (\varphi_{P3} + \varphi_{P4}),$ requiring mutual pump coherence to ensure the coherence of the superposition state. Subscript "Pi" denotes i<sup>th</sup> pump wave. This scheme represents a spatial-mode generalization of the Kwiat's original polarization-entanglement scheme [17] that used a sequence of two thin down-conversion crystals oriented with 90-degree angle between their optical axes, with pump at 45 degrees with respect to either axis. Just as there is no way to tell which crystal has produced a given photon pair, there is also no way to tell which of the two IM-FWM processes has produced a given photon pair, which results in generation of the superposition of the states yielded by the two processes. Energy conservation and phase matching conditions need to be satisfied for each process. Energy conservation laws for processes 1 and 2 are:

(Process 1) 
$$v_I = v_{P1} + v_{P2} - v_S$$
, (1)

(Process 2) 
$$v_I = v_{P3} + v_{P4} - v_S$$
, (2)

where  $\nu$  is the optical frequency for each wave. IM-FWM selection rules [18] require preservation of the total number of photons in each spatial mode for each process. The phase matching conditions are given by:

(Process 1) 
$$\beta^{(11a)}(\omega_I) = \beta^{(01)}(\omega_{P1}) + \beta^{(11a)}(\omega_{P2})$$
  
 $-\beta^{(01)}(\omega_S),$  (3)  
(Process 2)  $\beta^{(01)}(\omega_I) = \beta^{(01)}(\omega_{P3}) + \beta^{(11a)}(\omega_{P4})$   
 $-\beta^{(11a)}(\omega_S),$  (4)

where  $\beta$  is the propagation constant, and  $\omega = 2\pi \nu$ . Taylor expansion of  $\beta^{(i)}(\omega)$  reduces the phase-matching condition to

(Process 1) 
$$\beta_1^{(01)} \left( \frac{\omega_S + \omega_{P1}}{2} \right) = \beta_1^{(11a)} \left( \frac{\omega_I + \omega_{P2}}{2} \right),$$

(Process 2) 
$$\beta_1^{(01)} \left( \frac{\omega_I + \omega_{P3}}{2} \right) = \beta_1^{(11a)} \left( \frac{\omega_S + \omega_{P4}}{2} \right),$$
 (6)

where  $\beta_1$  denotes the inverse group velocity  $1/v_g$ .

Phase-matching conditions (5), (6) mean that, for each process, the group velocities at the average frequencies of the two waves present in each spatial mode must be equal [18]. These average frequencies, converted to wavelengths, are shown by the dashed lines in Fig. 1. Figure 2 shows measured relative inverse group velocities (RIGV)  $1/v_g$  of LP<sub>01</sub>, LP<sub>11a</sub>, and LP<sub>11b</sub> modes of our TMF. The LP<sub>11a</sub> and LP<sub>11b</sub> curves are approximately parallel to the LP<sub>01</sub> curve and are horizontally shifted from it by  $\sim$ 24 nm ( $\Delta v_1 = 3$  THz) and  $\sim$ 41 nm ( $\Delta v_2 = 5.1$  THz), respectively. Thus, phase matching is

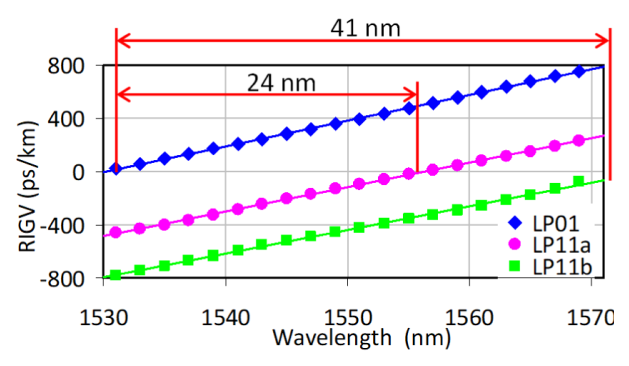


Fig. 2. Measured relative inverse group velocities (RIGVs) for our TMF modes.

satisfied when the dashed lines in Fig. 1 are separated by 24 nm, and we have:

(Process 1) 
$$\frac{v_S + v_{P1}}{2} - \frac{v_I + v_{P2}}{2} = \Delta v_1, \tag{7}$$

(Process 2) 
$$\frac{v_I + v_{P3}}{2} - \frac{v_S + v_{P4}}{2} = \Delta v_1.$$
 (8)

To satisfy energy conservation and phase-matching conditions for both processes simultaneously, we have solved the system of Eqs. (1), (2), (7), and (8), which has resulted in 4 constraints on the frequencies of the 6 involved waves:  $v_{P1(P3)} = v_{I(S)} + \Delta v_1$  and  $v_{P2(P4)} = v_{S(I)} - \Delta v_1$ . Here, one pair of two frequencies that are not separated by  $\Delta v_1$  can be arbitrarily chosen. In our experiment, we choose signal to be at 1571.9 nm and idler at 1561.5 nm, which results in pumps 1, 2, 3, and 4 placed at 1537.3, 1596.8, 1547.3, and 1586.2 nm, respectively.

In our scheme, two of the four pumps must be positioned on the short-wavelength side of the signal and idler, which leads to Raman photons generated even at zero temperature. To minimize Raman scattering, the TMF RIGV curves should ideally have the shift  $\Delta \nu_1$  that is significantly greater than Raman peak shift  $\Delta \nu_R = 13$  THz (this is not the case in our proof-of-concept experiment), which will place the signal and idler outside of Raman gain region of the pumps. At the same time, the RIGV curves should have a very low slope (small dispersion) to help minimize the group walk-off between the two modes. Further reduction of Raman scattering can be achieved by weakening the short-wavelength pumps and strengthening long-wavelength pumps while keeping their geometric average (responsible for parametric gain) the same.

The TMF group velocity dispersion in our setup leads to gradual walk-off among the 4 interacting waves in each process. The largest group walk-off is between the signal and idler waves in process 1, which in our case amounts to  $\sim$ 680 ps at the end of the fiber. For 10-ns-long pump pulses used in our experiment, this is equivalent to  $\sim$ 7% reduction in the state fidelity (from 100% to 93%), which could be improved by using shorter (or less dispersive) fiber and higher pump power.

Another potential source of entanglement degradation is the presence of two wavelength-conversion processes with conversion efficiencies  $\sim \langle n \rangle$ :  $\omega_{P1} + \omega_S = \omega_{P3} + \omega_I$  and  $\omega_{P2} + \omega_I = \omega_{P4} + \omega_S$ , which are phase-matched when pumps' mode is different from signal/idler mode. For the desired  $\langle n \rangle \leq 0.01$ , the low conversion efficiency of these processes cannot degrade the entanglement fidelity by more than 1%.

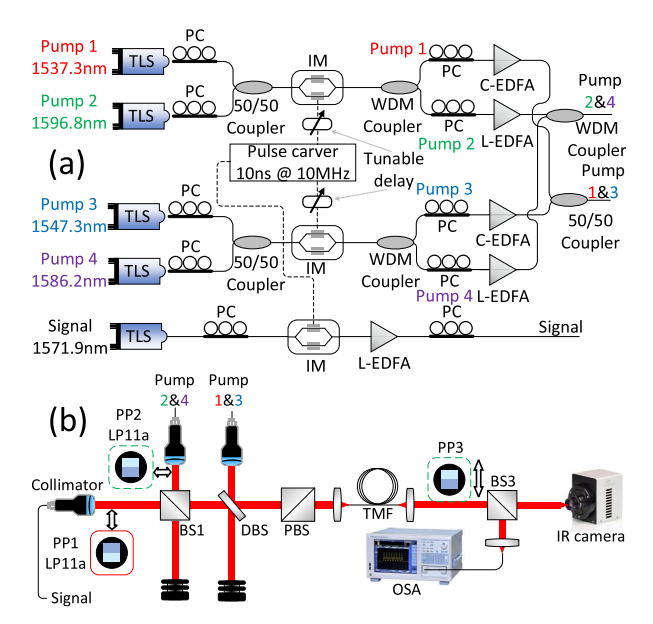


Fig. 3. Experimental setup: (a) pump and signal intensity modulation, synchronization, and amplification; (b) spatial-mode conversion, free-space coupling into the TMF, and output of the IM-FWM experiment.

#### III. EXPERIMENTAL SETUP

The experimental setup is shown in Fig. 3. As can be seen in Fig. 3a, the pumps 1–4 and signal are carved into 10-ns-long flat-top pulses with a 10-MHz repetition rate by 3 intensity modulators. The pumps are amplified by telecom-grade C- and L-band erbium-doped fiber amplifiers (EDFAs). Amplified pumps 1 and 3 are combined by a 50/50 coupler. Amplified pumps 2 and 4 are combined by a WDM coupler. In Fig 3b, pumps 2 and 4 are converted to LP<sub>11a</sub> mode by a phase plate PP2, combined with the signal by a free-space beam splitter BS1 and with pumps 1 and 3 by a free-space dichroic beam splitter DBS, and then coupled into the 1-km-long TMF by an objective. TMF output is collimated by a second objective. We split the output between an infrared camera and a single-mode fiber (SMF) connected to the optical spectrum analyzer (OSA), which in this case measures the LP<sub>01</sub> "output port" of the TMF. By inserting phase plate PP3 prior to the OSA's SMF input, we can also measure LP11a "output port" of the TMF. We can gradually vary the signal spatial mode from LP<sub>01</sub> to LP<sub>11a</sub> by vertically moving the phase plate PP1 (when it is centered on the beam, it generates LP<sub>11a</sub> mode; when it is far off the center, it leaves the mode in  $LP_{01}$ ; in the intermediate positions it generates various two-mode superpositions). To maximize IM-FWM, we co-polarize all three input waves in each process.

# IV. RESULTS AND DISCUSSION

Mode selectivity of each process separately is investigated by comparing the idler power generated by the classical seed signal in the "correct" mode (LP<sub>01</sub> for process 1, LP<sub>11a</sub> for process 2) to that generated by the signal in the "wrong" mode (LP<sub>11a</sub> and LP<sub>01</sub>, respectively). Figure 4a shows the process 1 spectra at the TMF's LP<sub>11a</sub> output port, exhibiting mode selectivity of 19 dB. Figure 4b shows the process 2 spectra at the TMF's LP<sub>01</sub> output port, exhibiting mode selectivity better than 9 dB. It is difficult to estimate the selectivity of process 2 more accurately, because the idler generated

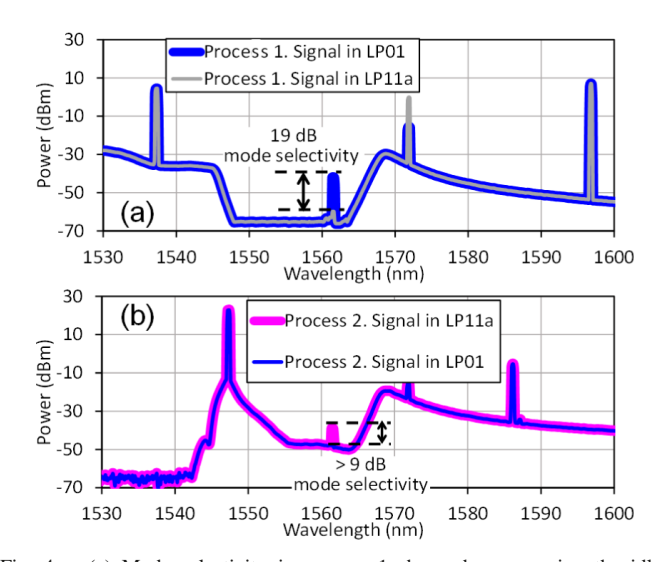


Fig. 4. (a) Mode selectivity in process 1 shown by comparing the idler generated at the  $LP_{11a}$  output port by the "correct" signal mode  $LP_{01}$  to that generated by the "wrong" mode  $LP_{11a}$ . (b) Mode selectivity in process 2 shown by comparing the idler generated at the  $LP_{01}$  output port by the "correct" signal mode  $LP_{11a}$  to that generated by the "wrong" mode  $LP_{01}$ .

by the "wrong" signal is buried deeply below the amplified spontaneous emission (ASE) noise from the pump EDFAs. We have observed mode selectivities better than 28 dB in [15], where we filtered ASE noise more aggressively.

Figure 5 shows spectra when all 4 pumps are present, i.e., both processes 1 and 2 taking place simultaneously. The results are measured at the  $LP_{01}$  output port (thick red) and  $LP_{11a}$  output port (thin blue) for signal in  $LP_{11a}$  mode. As expected, virtually no idler is present at the  $LP_{11a}$  port for such signal input (i.e., idler is deeply buried under the ASE noise). Average powers inside the TMF are 0 dBm for the signal and 20, 7.5, 20, and 9 dBm for pumps 1, 2, 3, and 4, respectively. In each process, the conversion efficiency is measured by comparing the powers of the idler and the original signal. The pump powers are chosen to equalize signal-to-idler CEs at -43 dB for processes 1 and 2.

With all 4 pumps present, Figure 6 shows the idler powers at the LP<sub>01</sub> and LP<sub>11a</sub> output ports for various two-mode superpositions of the input seed signal, after the ASE noise floor has been subtracted. One can see that, as the weight of LP<sub>11a</sub> signal mode in the superposition changes from 0 to 100%, the total idler power remains constant (within 1 dB), while the weights of idler modes LP<sub>01</sub> and LP<sub>11a</sub> change from nearly 0 to 100% and from 100% to nearly 0, respectively, as expected for the generated idler mode that is orthogonal to the input signal mode. In the future, we plan to stabilize the phase  $\Delta \varphi = (\varphi_{P1} + \varphi_{P2}) - (\varphi_{P3} + \varphi_{P4})$ , which would allow us to set the relative phase of the two modes in the idler mode superposition to make it perfectly orthogonal to the signal mode superposition. The mutual coherence of the 4 pumps can be obtained by deriving them from a common optical comb source. Any slow phase variations owing to differences in pumps' paths can be stabilized by using a fiber stretcher in one pump's path and monitoring one of the pumps' intensities at the TMF output. Since the same phase  $\Delta \varphi$  is also responsible for the direction of  $\omega_{P1} + \omega_{P2} = \omega_{P3} + \omega_{P4}$ phase-sensitive parametric amplification process among the 4 pumps (where either one photon of pump 1 and one photon

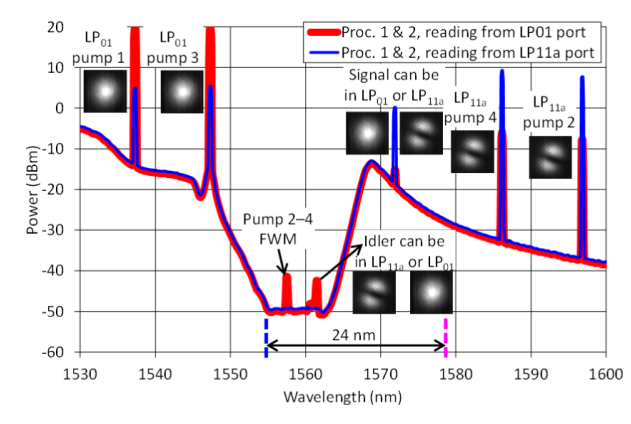


Fig. 5. Spectra for processes 1 and 2 occurring simultaneously, with seed signal in  $LP_{11a}$  mode, observed through  $LP_{01}$  (thick red) and  $LP_{11a}$  (thin blue) output ports. In addition, IM-FWM product of pumps 2, 3, and 4 appears at 1557.5 nm.

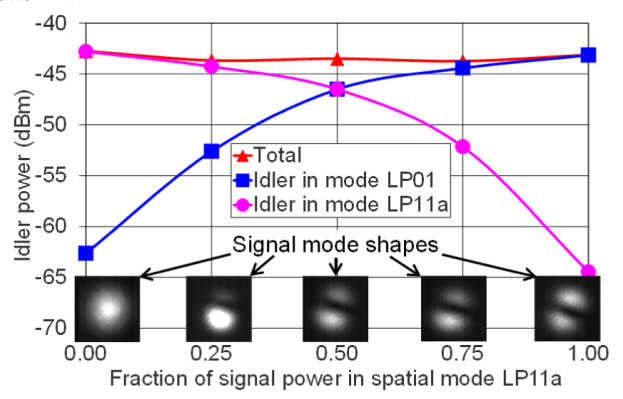


Fig. 6. Idler powers for various signal mode superpositions.

of pump 2 are annihilated while one photon of pump 3 and one photon of pump 4 are created, or vice versa), controlling the fiber stretcher to lock either maximum or minimum gain for the observed pump wave will lock the relative phase  $\Delta \varphi$ . Only one phase-locking loop is thus required.

## V. SUMMARY

Using a classical seed signal, we have demonstrated that a combination of two inter-modal four-wave-mixing processes in a few-mode fiber can couple a signal in an arbitrary twomode superposition to an idler in the orthogonal mode. The next step, apart from phase stabilization, will be to observe this mode anticorrelation in the single-photon regime (i.e., without the seed signal), which will require ~95-dB suppression of amplified spontaneous emission in the pump beams, as well as narrow-band signal and idler filtering to eliminate outof-band Raman noise (previously straightforwardly achieved by us with off-the-shelf components [19, 20]). Suppressing the in-band Raman noise, however, would require a customized FMF with  $\Delta v_1$  significantly exceeding 13 THz. In addition, separation or suppression of 4 pump waves after the TMF is required at  $\sim$ 140-dB level. If the signal at the output of TMF is to be transmitted over FMF-based link, then the pumps can be suppressed by 30–50 dB using several fiber Bragg gratings prior to entering the link, to bring their powers sufficiently low to avoid generating any noticeable Raman noise in the transmission fiber. The remaining pump separation / suppression can be done at the receiver side. While the scheme described in this paper can lead to generation of

spatial-mode entanglement in (LP<sub>01</sub>, LP<sub>11a</sub>) mode space of a few-mode fiber, a recently proposed alternative few-mode-fiber-based scheme [21] may similarly result in generation of entanglement in optical angular momentum space.

### REFERENCES

- A. Mair, A. Vaziri, G. Weihs, and A. Zeilinger, "Entanglement of the orbital angular momentum states of photons," *Nature*, vol. 412, no. 6844, pp. 313–316, Jul. 2001.
- [2] A. Sit et al., "High-dimensional intracity quantum cryptography with structured photons," Optica, vol. 4, no. 9, pp. 1006–1010, Aug. 2017.
- [3] W. Löffler, T. G. Euser, E. R. Eliel, M. Scharrer, P. S. J. Russell, and J. P. Woerdman, "Fiber transport of spatially entangled photons," *Phys. Rev. Lett.*, vol. 106, no. 24, Jun. 2011, Art. no. 240505.
- [4] Y. Kang, J. Ko, S. M. Lee, S.-K. Choi, B. Y. Kim, and H. S. Park, "Measurement of the entanglement between photonic spatial modes in optical fibers," *Phys. Rev. Lett.*, vol. 109, no. 2, Jul. 2012, Art. no. 020502.
- [5] N. H. Valencia, S. Goel, W. McCutcheon, H. Defienne, and M. Malik, "Unscrambling entanglement through a complex medium," *Nature Phys.*, vol. 16, no. 11, pp. 1112–1116, Aug. 2020.
- [6] H. Cao et al., "Distribution of high-dimensional orbital angular momentum entanglement over a 1 km few-mode fiber," Optica, vol. 7, no. 3, pp. 232–237, Mar. 2020.
- [7] D. Cozzolino et al., "Air-core fiber distribution of hybrid vector vortexpolarization entangled states," Adv. Photon., vol. 1, no. 4, Aug. 2019, Art. no. 046005.
- [8] F. Parmigiani et al., "All-optical mode and wavelength converter based on parametric processes in a three-mode fiber," Opt. Exp., vol. 25, no. 26, pp. 33602–33609, Dec. 2017.
- [9] O. F. Anjum et al., "Broadband study of inter-modal Bragg scattering four wave mixing in multi-mode fibres," in Proc. Eur. Conf. Opt. Commun. (ECOC), Rome, Italy, Sep. 2018, pp. 1–3, doi: 10.1109/ECOC. 2018.8535446.
- [10] E. Nazemosadat, A. Lorences-Riesgo, M. Karlsson, and P. A. Andrekson, "Design of highly nonlinear few-mode fiber for C-band optical parametric amplification," *J. Lightw. Technol.*, vol. 35, no. 14, pp. 2810–2817, Jul. 15, 2017.
- [11] K. Rottwitt, J. Koefoed, and E. Christensen, "Photon-pair sources based on intermodal four-wave mixing in few-mode fibers," *Fibers*, vol. 6, no. 2, p. 32, May 2018.
- [12] C. Guo, J. Su, Z. Zhang, L. Cui, and X. Li, "Generation of telecomband correlated photon pairs in different spatial modes using few-mode fibers," Opt. Lett., vol. 44, no. 2, pp. 235–238, Jan. 2019.
- [13] K. Sulimany and Y. Bromberg, "All-fiber source and sorter for multi-mode correlated photons," 2020, arXiv:2012.14024. [Online]. Available: http://arxiv.org/abs/2012.14024
- [14] D. Cruz-Delgado et al., "Fiber-based photon-pair source capable of hybrid entanglement in frequency and transverse mode, controllably scalable to higher dimensions," Sci. Rep., vol. 6, no. 1, Jun. 2016, Art. no. 27377.
- [15] A. Shamsshooli, C. Guo, F. Parmigiani, X. Li, and M. Vasilyev, "Toward generation of spatially-entangled photon pairs in a few-mode fiber," in *Proc. CLEO Conf.*, San Jose, CA, USA, May 2020, Paper JTh2A.27.
- [16] A. Shamsshooli, C. Guo, M. Vasilyev, F. Parmigiani, and X. Li, "Progress toward generation of spatially-entangled photon pairs in a few-mode fiber," in *Proc. IEEE Photon. Conf. (IPC)*, Sep. 2020, pp. 1–2, Paper MI2.2, doi: 10.1109/IPC47351.2020.9252314.
- [17] P. G. Kwiat, E. Waks, A. G. White, I. Appelbaum, and P. H. Eberhard, "Ultra-bright source of polarization-entangled photons," *Phys. Rev. A*, *Gen. Phys.*, vol. 60, no. 2, pp. R773–R776, Aug. 1999.
- [18] R.-J. Essiambre et al., "Experimental investigation of inter-modal four-wave mixing in few-mode fibers," *IEEE Photon. Technol. Lett.*, vol. 25, no. 6, pp. 539–542, Mar. 15, 2013.
- [19] Y. B. Kwon *et al.*, "Experimental demonstration of spatial-mode-selective frequency up-conversion in a multimode  $x^{(2)}$  waveguide," in *Proc. CLEO Conf.*, San Jose, CA, USA, Jun. 2016, Paper STh3P.4.
- [20] Y. B. Kwon, M. Giribabu, C. Langrock, M. M. Fejer, and M. Vasilyev, "Single-photon-level spatial-mode-selective frequency up-conversion in a multimode x<sup>(2)</sup> waveguide," in *Proc. CLEO Conf.*, San Jose, CA, USA, May 2017, Paper FF2E.1.
- [21] A. Shamsshooli, C. Guo, F. Parmigiani, X. Li, and M. Vasilyev, "Toward generation of orbital-angular-momentum-entangled photon pairs in a few-mode fiber," in *Proc. Frontiers Opt./Laser Sci.*, 2020, pp. 1–2, Paper FM1D.2, doi: 10.1364/FIO.2020.FM1D.2.